5.5   COMPARISON OF POLARIMETRIC RADAR OBSERVATIONS OF TORNADIC SUPERCELLS AT S, C, AND X BANDS

MATTHEW KUMJIAN[1,2,3], JEFF SNYDER[2], ALEXANDER RYZHKOV[1,3], DUŠAN ZRNIĆ[3], STEVE FRASIER[4], AND HOWIE BLUESTEIN[2]

1.   Cooperative Institute of Mesoscale Meteorological Studies, Norman, Oklahoma
2.   School of Meteorology, University of Oklahoma, Norman, Oklahoma
3.   National Severe Storms Laboratory, Norman, Oklahoma
4.   Department of Electrical Engineering, University of Massachusetts, Amherst, Massachusetts

1.   INTRODUCTION

Early studies of tornadic supercell storms have relied heavily on weather radar and Doppler radar observations, which garnered invaluable information regarding the structure and airflow patterns within such storms. Microphysical research was limited, however, because conventional single-polarization radar measurements are inadequate for microphysical retrievals and most existing storm-scale models use simplified bulk parameterization schemes.

Dual-polarization radar observations provide remarkable insight into the microphysics of severe convective storms. The use of radar signals at orthogonal polarizations reveals information about the size, shape, composition, orientation, and diversity of scatterers within the sampling volume. Recent research on tornadic supercells utilizing polarimetric radars has revealed distinct and intriguing signatures regarding storm evolution and severity, including the tornadic debris signature (TDS; Ryzhkov et al. 2002, 2005a), the low-level Z_{DR} arc, Z_{DR} and K_{DP} columns, midlevel Z_{DR} and ρ_{HV} rings, and the updraft signature (Kumjian and Ryzhkov 2008). Van Den Broeke et al. (2008) and Romine et al. (2008) have looked at the evolution of such polarimetric features in tornadic supercells in detail.

Because of the advantages offered by polarimetric data, the upcoming VORTEX2 field campaign is expected to rely heavily on polarimetric measurements collected at S, C, and X bands (Markowksi 2008, personal communication). Studies have investigated polarimetric data at S, C, and X bands independently, but so far none have compared observations of tornadic supercells at three different radar wavelengths. Herein we investigate similarities and differences in the data from tornadic supercells at S band (from central Oklahoma), C band (from Enterprise, Alabama), and X band (from western Oklahoma and southwestern Kansas). Though a direct comparison of the same storm is not yet available, the consistent appearance of certain features in supercells allows for a unique analysis of microphysics enhanced with the indirect comparisons of these multiwavelength polarimetric data.

The purpose of this paper is to highlight similarities and differences in polarimetric observations of tornadic supercells at various wavelengths and to raise important issues regarding data collection, quality, and interpretation that should be considered before embarking on the forthcoming field program. In the next section we briefly describe the radar systems and datasets that we employ in this study. Section 3 provides an analysis of the data and a discussion concerning its interpretation, problems, and other issues. We conclude with a brief summary and recommendations in Section 4.

2. RADAR SYSTEMS AND DATA OVERVIEW

Data from three polarimetric radar systems are analyzed in this study. S-band measurements come from the research polarimetric prototype WSR-88D in Norman, Oklahoma, operated by the National Severe Storms Laboratory (KOUN). Data at C band are from the Enterprise Electronics Corporation "Sidpol" radar in Enterprise, Alabama. X-band data come from the University of Massachusetts mobile "X-Pol" radar operated by students and faculty at the University of Oklahoma.

Each radar was operated using simultaneous transmission of linear orthogonal polarized signals. This allows for the estimation of radar reflectivity factor at horizontal polarization (Z_H), differential reflectivity (Z_{DR}), differential phase (Φ_{DP}) and specific differential phase (K_{DP}), and the co-polar cross-correlation coefficient at zero lag (ρ_{HV}). Selected details of the radar systems are provided in Table 1.

Radar	Wave-length	Peak Power	3-dB Beamwidth	Range Resolution
KOUN	10.9 cm	750 kW	0.95°	267, 250 m
Sidpol	5.3 cm	250 kW	1.0°	125 m
X-Pol	3.2 cm	25 kW	1.25°	150 m

Table 1: Selected details of the radar systems utilized in this study.

3. ANALYSIS AND DISCUSSION

3.1. *Polarimetric Signatures*

Because of the scattering properties of hydrometeors at different radar wavelengths, one should expect both similarities and differences in polarimetric signatures at S, C, and X bands. For example, tornadic debris has electromagnetic properties very distinct from hydrometeors because of its irregular shape, random orientation, variable dielectric constant, and often large size. Polarimetric measurements of tornadoes reveal such debris as the TDS, marked by high Z_H and anomalously low ρ_{HV} (and sometimes near-zero Z_{DR}). The TDS has been observed numerous times at S band (Giangrande 2002; Ryzhkov et al. 2002, 2005a; Schuur et al. 2004; Kumjian and Ryzhkov 2008; Schenkman et al. 2008), C band (Outinnen and Teittinen 2007, 2008; Kumjian et al. 2008), and X band (Lopez et al. 2004; Junyent et al. 2005; Bluestein et al. 2007).

Another signature that is consistently observed at all radar wavelengths is the Z_{DR} arc, a narrow arc-shaped region of very high (> 4 dB) Z_{DR} values located along the edge of the forward-flank precipitation echo and inflow region. Since the Z_{DR} arc likely originates from size sorting due to strong inflow and veering wind shear characteristic of supercells and their environments (Kumjian and Ryzhkov 2009), we expect the observed consistency of the signature. Subtle differences do exist, however, in the magnitude of the Z_{DR} arc owing to differences in scattering properties of large raindrops (> 5 mm) at the different radar wavelengths, notably the resonance scattering effects that will be discussed later. The magnitude of Z_{DR} in the arcs is larger at C and X band, sometimes exceeding 5 – 6 dB. Examples of Z_{DR} arcs in storms at different radar wavelengths are shown in Fig. 1. Interestingly, as the radar resolution increases, the Z_{DR} arc is observed to be thinner. Snyder (2008) reports it being less than 500-m wide in a case he investigated.

One of the best known benefits of polarization diversity is the discrimination of hydrometeor species, such as rain, snow, hail, etc. Hail detection with S-band polarimetric radars has been thoroughly explored and validated (e.g., Ryzhkov et al. 2005b; Heinselman and Ryzhkov 2006). In supercell storms, the hail signature – that is, high Z_H collocated with low Z_{DR} – is frequently observed at S band, especially in nontornadic supercells (Kumjian and Ryzhkov 2008). This is because large hail tends to tumble when it falls, resulting in isotropic scattering, which drives Z_{DR} to zero. However, at C and X bands, resonance scattering effects from larger raindrops (> 4 mm) and smaller melting hail tends to overwhelm the backscattered signal. Because raindrops have higher dielectric constant and are oblate in shape, these properties dominate the contributions to the sampling volume, resulting in high Z_{DR}. As discussed in Ryzhkov et al. (2007) and Kumjian and Ryzhkov (2008), the hail signature may not appear at C band. A thorough examination of numerous cases at X band (Snyder 2008) also suggests that the hail signature may not be common, if it appears at all.

Z_{DR} and K_{DP} columns have been noted extensively in the literature owing to their prevalence in convective storms. Such columns of enhanced Z_{DR} values are evident in data from all three wavelengths. At C band, these columns could be even more prominent, with larger Z_{DR} magnitudes and greater areal extent due to resonance effects of large raindrops and smaller melting hail. K_{DP} estimates at X band require careful editing of Φ_{DP} measurements, which are not available for all the X-band datasets. Thus, we cannot adequately compare the appearance of K_{DP} columns in tornadic storms. However, we anticipate that K_{DP} columns should be observable at all wavelengths, again being particularly prominent at C band as well as X band. We also expect a similar misalignment of the K_{DP} and Z_{DR} columns in supercells as noted by several authors (e.g., Hubbert et al. 1998; Loney et al. 2002; Schlatter 2003; Ryzhkov et al. 2005a; Kumjian and Ryzhkov 2008; Romine et al. 2008). It is important to obtain multiwavelength measurements of K_{DP} columns as they are associated with the supercell rear-flank downdrafts.

Midlevel rings of enhanced Z_{DR} and reduced ρ_{HV} are frequently observed at S band in supercells between 3 – 6 km AGL (Kumjian and Ryzhkov 2008) and are thought to originate from melting hail and graupel in and on the edge of the updraft being wrapped around cyclonically by the mesocyclone. Midlevel rings or half-rings have possibly been observed at C band and X band, though so far the observations are limited (Figs. 2 – 3). A dual-Doppler analysis of a tornadic supercell by Payne et al. (2008) confirmed that the cyclonic vorticity maximum was collocated with the center of a midlevel ρ_{HV} ring (observed at S band). Since these signatures are likely resulting from larger raindrops and melting hail particles, more pronounced resonance effects at smaller wavelengths may cause subtle differences in the alignment, thickness, and location of these features.
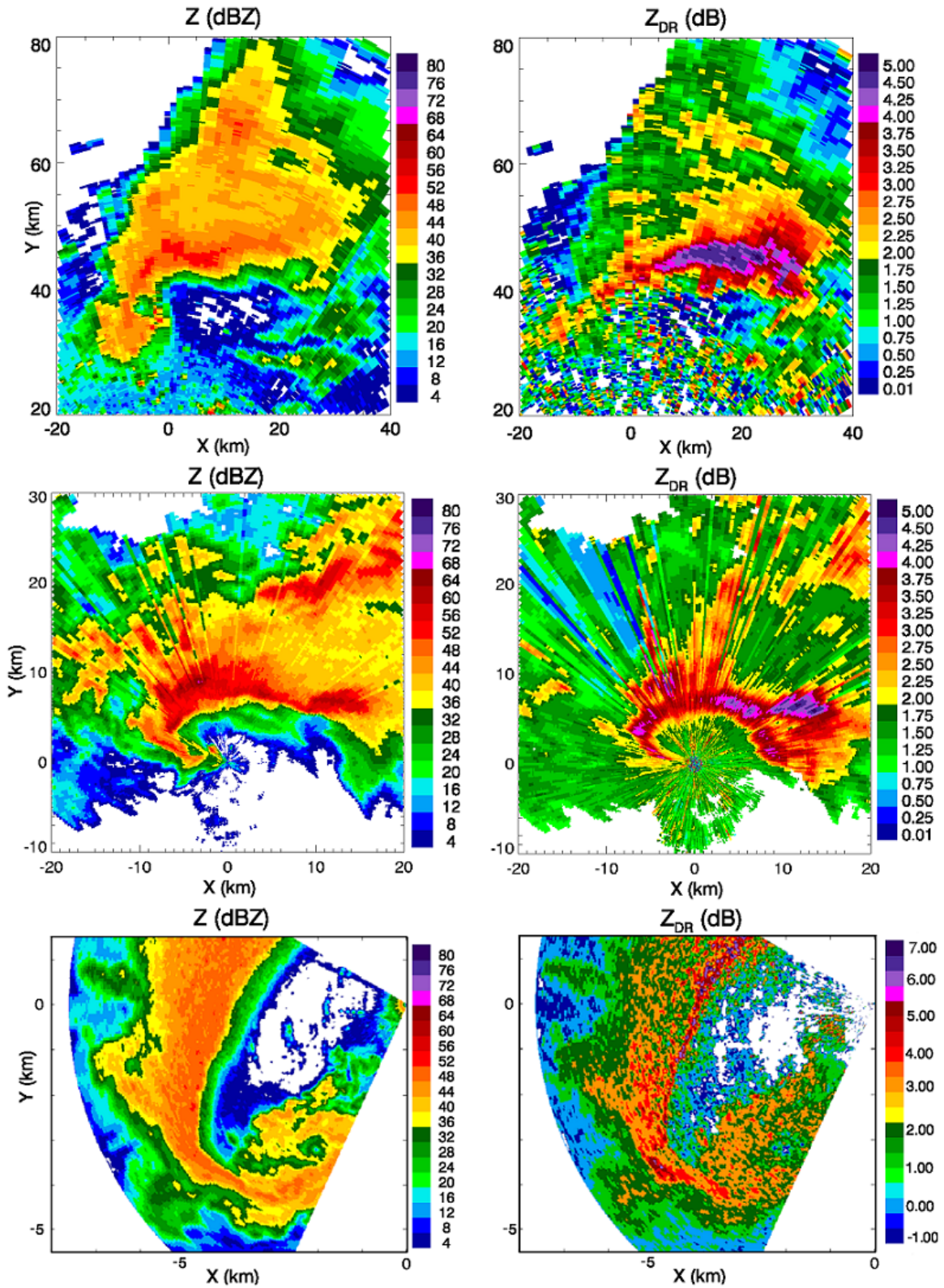
Fig. 1: PPI fields of Z_H and Z_{DR} depicting several examples of Z_{DR} arcs at different radar wavelengths. From top to bottom: 10 May 2003, 0333 UTC at 0.5° elevation (S band); 1 March 2007, 1912 UTC at 5° elevation (C band); 13 May 2004, 0121 UTC at 3° elevation (X band).
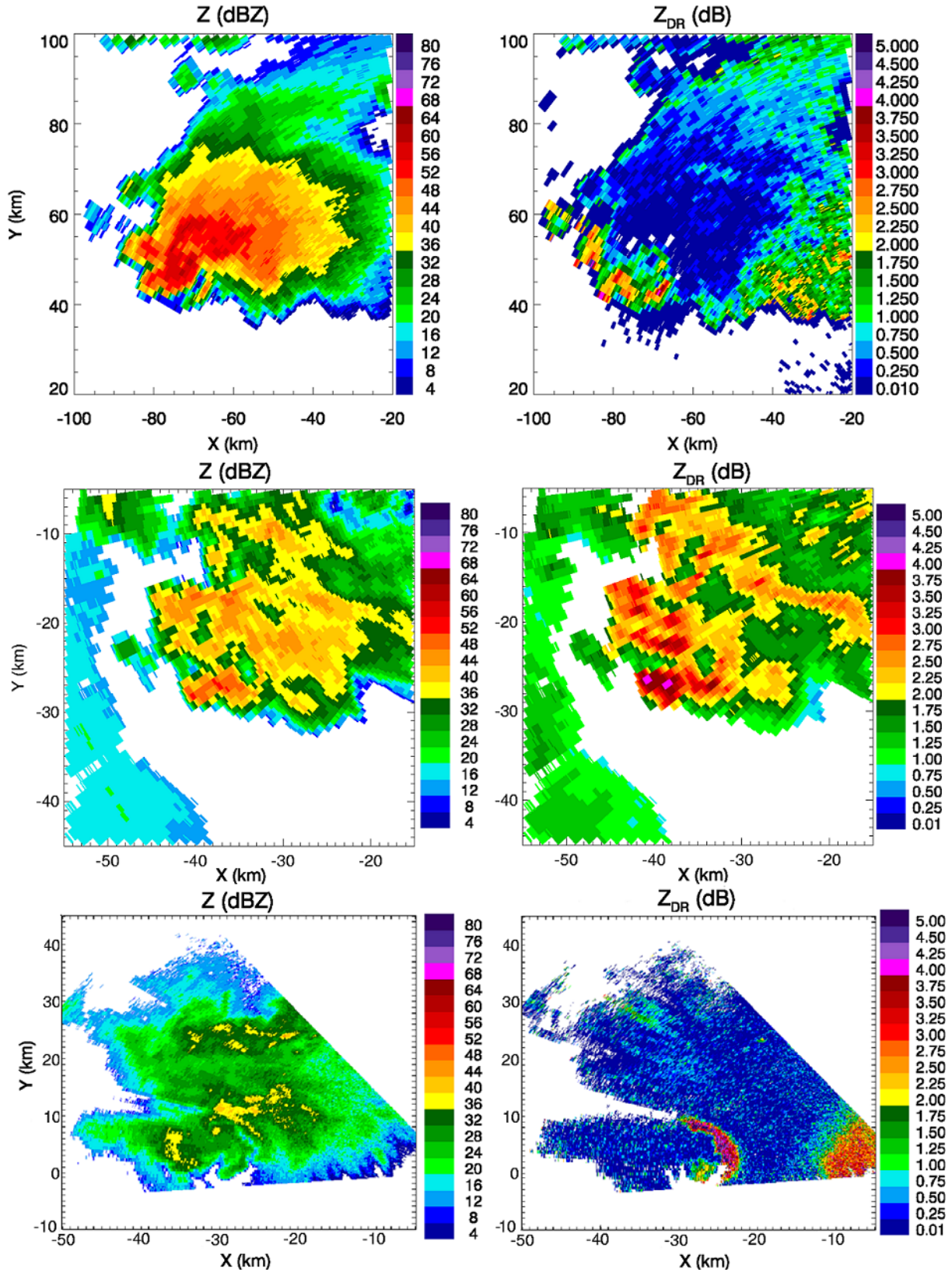
Fig. 2: Examples of Z_{DR} rings and half rings at different radar wavelengths. From top to bottom: 30 May 2004, at 0044 UTC, 2.5° elevation (S band); 1 March 2007, at 1827 UTC, 5.5° elevation (C band); 31 May 2007, at 2344 UTC, 11.9° elevation (X band). In each, the left panel is Z_H, the right panel Z_{DR}.
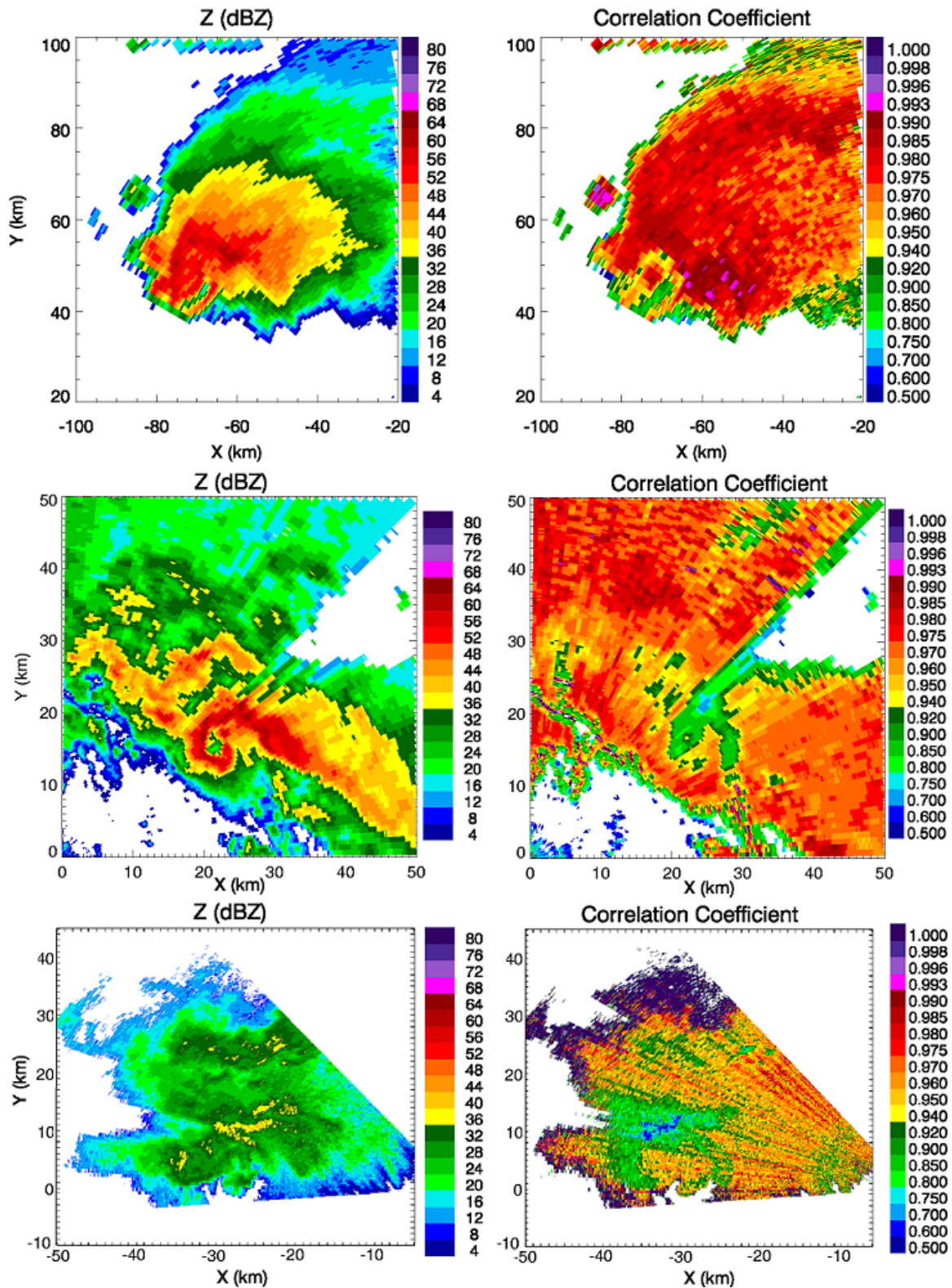
Fig. 3: As in Fig. 2, except examples of ρ_{HV} rings and half rings are shown. From top to bottom: 30 May 2004 at 0044 UTC, 3.5° elevation (S band); 1 March 2007, at 1932 UTC, 6.5° elevation (C band); 31 May 2007, at 2342 UTC, 11.2° elevation (X band).

3.2. *Attenuation and Correction Techniques*

Weather radar data tend to be affected by attenuation from several sources: precipitation-sized particles, atmospheric gases, water vapor, and cloud water. Even at X band, however, specific attenuation by oxygen and water vapor is approximately 0.0095 and 0.003 dB km^{-1}, respectively (Van Vleck 1947a, 1947b). Given the mobility of the UMass X-Pol, data collected by this radar tend to be within 20-25 km of the radar, a distance over which the total attenuation by atmospheric gases is negligible. In addition, the radar operators attempt to collect data as close to the ground as possible so as to collect data under cloud base. As such, for the X-band attenuation-corrected data used in this study, the effects of attenuation by atmospheric gases and cloud water are ignored.

Attenuation and differential attenuation are a function of, among other factors, radar wavelength. Specific attenuation (A_H) and specific differential attenuation (A_{DP}) are larger for shorter wavelengths because: (i) they are inversely proportional to radar wavelength, and (ii) the imaginary part of the complex dielectric constant ε is higher at shorter wavelengths for a given temperature. In general, attenuation at X band is expected to be nearly two orders of magnitude larger than at S-band and up to an order of magnitude larger than at C band. To be able to properly interpret Z_H and Z_{DR} data, even in a qualitative sense, it becomes increasingly important to correct for the effects of attenuation when examining C-band and, especially, X-band radar data. An example of severe attenuation and signal extinction before the end of the cell is provided in Figure 4.

Correction for attenuation of radar reflectivity factor data requires an estimate of specific attenuation or path-integrated attenuation. Bringi et al. (1990) found that A_H and A_{DP} are nearly linearly related to

K_{DP}; there exists a relationship between K_{DP} and A_H of the form

$$A_H = \alpha_H K_{DP}{}^{\beta_H} \qquad (1)$$

where the exponent β_H is typically assumed to be unity. The use of K_{DP} in the estimation of attenuation is more stable than the use of only Z_H in the A_H-Z_H relationship (Bringi et al. 1990), which is one significant benefit of polarimetric weather radar. Ryzhkov and Zrnić (1995) and Carey et al. (2000) calculated an equivalent α_H by finding the best-fit line of range profiles of Z_H vs. Φ_{DP} at S band and C band, respectively. Such a technique is best suited for homogeneous stratiform precipitation, a characteristic not common in supercells. The A_H-K_{DP} relationship as a technique for estimating attenuation was extended by Testud et al. (2000) by using it to estimate the total path-integrated attenuation (PIA) for use in the ZPHI rain-profiling algorithm, a technique that apportioned PIA according to the observed Z_H profiles. Both the original differential phase method and the later ZPHI technique rely on choosing a fixed constant in the A_H-K_{DP} relationship, the true value of which may actually change as the drop-size distribution changes. To ameliorate this impediment, Bringi et al. (2001) developed the Self-Consistent with Constraints (SCWC) technique wherein the constant of proportionality is calculated by the observed differential phase data.

As with attenuation, there exist several methods by which to estimate differential attenuation, including a relatively straightforward relationship between A_{DP} and K_{DP} (Bringi et al. 1990):

$$A_{DP} = \alpha_{DP} K_{DP}{}^{\beta_{DP}} \qquad (2)$$

Others have used a linear relationship between A_{DP} and A_H. In addition, Liu et al. (2006) obtained attenuation-corrected Z_{DR} by correcting both Z_H and Z_V according to the SCWC technique, recalculating Z_{DR} based on the attenuation-corrected Z_H and Z_V.
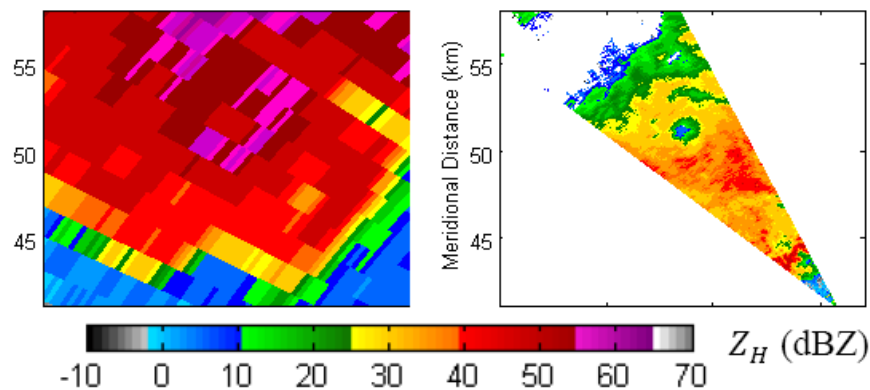

Figure 4: Z_H data of the hook echo and rear-flank downdraft region of a high-precipitation supercell valid at 0055 UTC on 30 May 2004. (a) Data from KOUN valid at a 0° elevation angle; (b) data from the UMass X-Pol valid at the same time at an elevation angle of 5.1°.

It must be noted that data collected by the UMass X-Pol radar over the past several years reveal that the complete extinction of the radar signal (i.e., the point at which the returned signal drops below the minimum detectable signal) can occur over path lengths of as little as 8 km. The attenuation correction techniques presented by previous authors and examined in Snyder (2008) are only able to provide an estimate of path-integrated attenuation in areas with detectable signal. As such, in those cases in which the signal power drops to the noise floor before the signal is able to travel beyond the supercell, attempts at determining storm structures or characteristics addressed in this manuscript become impossible. In addition, an accurate estimate of K_{DP} requires the removal of backscatter differential phase (δ) from the total differential phase; K_{DP} should be calculated from the differential propagation phase, lest changes in backscatter differential phase may obfuscate K_{DP}. The estimate of Φ_{DP} from the UMass X-Pol data was obtained by filtering the measured total differential phase in a manner similar to that of Hubbert and Bringi (1995). Even with this filtering, it is often difficult to remove completely δ, particularly when δ is present over distances longer than a couple of kilometers.

In supercell hail cores, Ryzhkov et al. (2007) has looked at relatively localized regions of significant anomalous differential attenuation, which they called "hot spots." In this case, the majority of the path-integrated differential attenuation occurs on very small spatial scales, and thus traditional methods of correcting differential attenuation that assume fixed constants in the A_{DP}-K_{DP} relationship are inadequate. In such cases, the hot spots must be identified, δ removed, and the constant of proportionality determined by the method discussed in Ryzhkov et al. (2007).

3.3. *Multiwavelength Scattering and Resonance Effects*

An important question when it comes to directly comparing multiwavelength polarimetric data is whether or not the observed values of the polarimetric variables should be same at S, C, and X band. This has implications for absolute calibration issues. For example, the research radar KOUN is calibrated by comparing the reflectivity factor values to that of the nearby operational National Weather Service WSR-88D in Twin Lakes, Oklahoma (KTLX), which also operates at S band. One can calibrate a radar by using another nearby radar operating at the same frequency, but not by comparing two radars operating at different frequencies. We can further explore this issue using observations and theoretical calculations, such as the T-matrix method of calculating complex scattering amplitudes.

Early studies of dry and wet ice cores found that the backscattered cross section is generally *not* the same for different incident wave frequencies (Atlas and Ludlam 1961; Fig. 5). Recall that the backscattering cross-section is defined as

$$\sigma_{a,b} = 4\pi \left| f_{a,b}^{(\pi)} \right|^2 \qquad (3)$$

where in the Rayleigh approximation, the complex forward and backwards scattering amplitudes are equivalent: $f_{a,b}^{(\pi)} = f_{a,b}^{(0)} \propto \lambda^{-2}$. Thus, $\sigma_{a,b} \sim \lambda^{-4}$. Since reflectivity factor is defined as

$$Z_H = \frac{4\lambda^4}{\pi^5 |K_w|^2} \int_0^\infty \left| f_b^{(\pi)} \right|^2 N(D)dD \qquad (4)$$

it follows that Z_H should not depend on radar wavelength in the Rayleigh approximation. But when does the Rayleigh approximation hold and when does it break down?

For S-band radars, most hydrometeor sizes (including all raindrops) satisfy the Rayleigh approximation since the radar signal wavelength is much larger than the diameter of the particles. However, for radars operating with shorter wavelengths, this approximation breaks down for particular large sizes in which resonance scattering effects occur. Resonance scattering refers to the oscillation of the electromagnetic wave around the surface of the drop, which can constructively or destructively interfere with the backscattered signal. Such a scattering regime is dependent on the effective dielectric constant of the hydrometeor ε, radar wavelength λ, and the diameter of the particle itself (D). One can define the resonance parameter

$$\Re = \frac{D\sqrt{|\varepsilon|}}{\lambda} \qquad (5)$$

that approaches unity at the onset of resonance scattering effects. It should be noted that the Mie scattering solutions start to deviate from the Rayleigh solutions prior to the onset of resonance scattering effects. For rain, the Mie solutions start to diverge for $\Re \sim 0.5$. For pure ice, the solutions begin to diverge for $\Re \sim 0.3$. At X band, then, the Rayleigh approximation begins to break down for raindrops as small as $1 - 2$ mm in diameter, so most raindrops are *not* Rayleigh scatterers at X band (as are drops larger than about $3 - 4$ mm at C band). Therefore, we should expect similar differences in Z_H, Z_{DR}, and ρ_{HV} in both rain and hail.

Ryzhkov and Zrnić (2005) showed from theoretical calculations that the measured Z_H, Z_{DR}, K_{DP}, and ρ_{HV} will be different depending on radar wavelength. For liquid raindrops at $T = 20$ °C, the Z_{DR} and K_{DP} at S, C, and X bands are shown in Figure 6. Perhaps most striking is the large difference in Z_{DR} at C band for
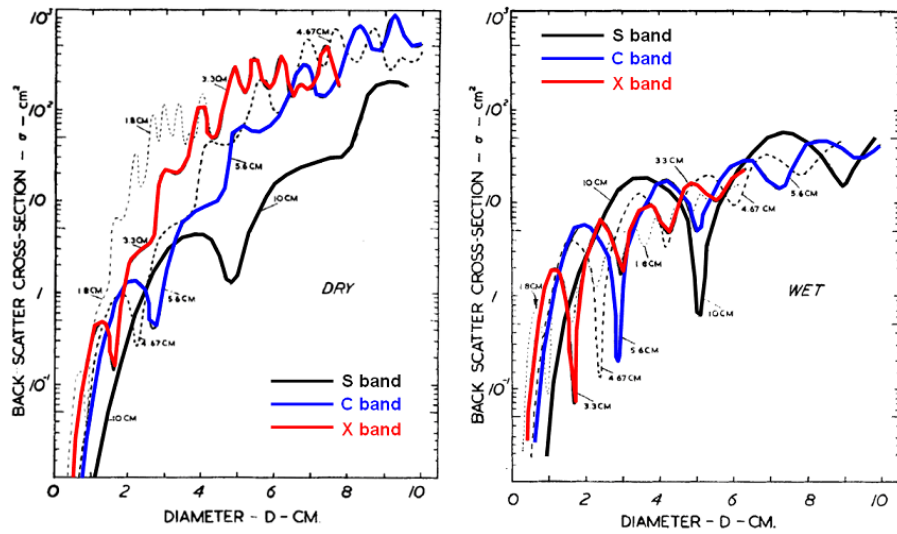
Fig. 5: The backscatter cross-section (cm²) for ice spheres that are dry (left panel) and wet (right panel) for different radar frequencies. The S, C, and X-band curves are highlighted in thick black, blue, and red, respectively. Adapted from Atlas and Ludlam (1961).
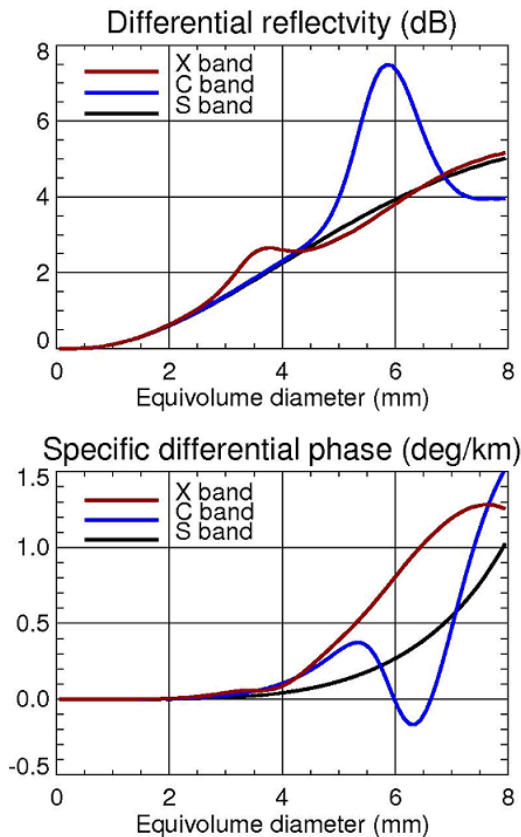

Fig. 6: Calculated values of Z_{DR} in dB (top) and K_{DP} in deg km⁻¹ (bottom) as a function of raindrop equivolume diameter in mm for S, C, and X bands (black, blue, and red curves, respectively) for a temperature of 20 °C. Adapted from Ryzhkov and Zrnić (2005).

large raindrops. This is a very clear manifestation of resonance scattering effects. These resonance effects are not as pronounced at X band due to greater attenuation of the signal within the drop. Resonance scattering can also explain the observation that pure rain at C band can have ρ_{HV} as low as 0.93, much lower than observed at S band or X band.

Particles for which resonance scattering effects occur (herein "resonance scatterers") are characterized by significant differential phase upon backscatter (δ). Note that ρ_{HV} is strongly affected by the relative contribution from resonance scatterers since the formula contains δ in the numerator:

$$\rho_{HV} = \frac{\left| \left\langle \sqrt{\sigma_H} \sqrt{\sigma_V} e^{i\delta} \right\rangle \right|}{\sqrt{\left\langle \sigma_H \right\rangle} \sqrt{\left\langle \sigma_V \right\rangle}} \quad (6)$$

At S band, the resonance size for a pure raindrop would be on the order of 1.1 cm, which does not occur naturally. This is why δ in pure rain at S band is negligible. However, at shorter wavelengths the resonance scatterers include large raindrops (4 – 6 mm at C band; 3-5 mm at X band). Since raindrops of this size are common in convective storms, resonance scattering effects are prevalent in observations at C and X bands. Since the radar signal attenuates more rapidly at X band, the resonance effects are most prominent at C band. This helps explain why in pure rain at C band ρ_{HV} can drop as low as 0.93; if a substantial number of large raindrops (with nonzero δ) contribute to the backscattered signal, ρ_{HV} will drop significantly.

In addition to decreasing ρ_{HV}, resonance scattering effects can substantially affect the measured Z_{DR} and

K_{DP} (especially at C band). This is why polarimetric signatures in supercells may be more prominent at C band than at S band, especially those in fields of Z_{DR}. Also note that K_{DP} can become negative for resonance scatterers at C band (Fig. 6), which can cause problems for rainfall estimation and attenuation correction.

3.4. *Accounting for large antenna elevation angles*

As a benefit of their portability, small mobile radars are often taken very close to the storms that they are observing. This strategy results in very high-resolution low-level data that is important for studies of tornadoes and hook echoes (e.g., Bluestein et al. 2007). However, if the goal is to collect volumetric data of supercell storms, such close range is not without a cost. To adequately sample a supercell to the height of 6-8 km, given a radar-to-storm distance on the order of 10-20 km, mobile radars often are operated at elevation angles up to 40°. At such steep angles, the direction of radar beam propagation is not quasi-parallel to the surface. Since raindrops tend to have canting angles of less than 10° – 20°, observing them with higher elevation angles cause the beam-relative aspect ratio of even large raindrops to trend much closer to unity than is typically encountered. Thus, the measured Z_{DR} and K_{DP} will *decrease* (towards 0 dB and 0 deg km^{-1}, respectively) with increasing elevation angle. On the other hand, the measured ρ_{HV} will *increase* for rain when observed with high look angles. Those interpreting polarimetric data and attempting hydrometeor classifications or other quantitative analyses should take this circumstance into account.

3.5. *Other data concerns*

In addition to the issues discussed so far in this section, shorter wavelength radar systems have a few more concerns that must be addressed before the data are used and interpreted. Ryzhkov (2007) shows that the effects of nonuniform beam filling (NBF) are greater for shorter radar wavelengths. When the radar sampling volume encounters strong cross-beam gradients of differential phase Φ_{DP}, ρ_{HV} is negatively biased. Z_{DR} is affected by gradients of Z_H and Z_{DR}, but not Φ_{DP}. Therefore, NBF can either negatively or positively bias Z_{DR}, as described in detail in Ryzhkov (2007). Differential phase itself is inversely proportional to radar wavelength, so data processing techniques should account for situations in which Φ_{DP} folds or wraps from 360° or 180° back to zero.

In the presence of a strong electric field, as is common in the upper regions of supercell storms, ice crystals tend to become preferentially aligned. Radar systems that simultaneously transmit horizontal and vertical polarized waves are susceptible to depolarization of the transmitted signal, which happens as a result of cross-coupling induced by the oriented ice crystals, as demonstrated by Ryzhkov and Zrnić (2007). This causes radial "streaks" of alternating positive and negative Z_{DR}. Though such a signature serves as an indication of electrification and the presence of crystals, once depolarization occurs the signal becomes unusable and thus the data are lost for the rest of the radial. The effect should be more prominent at shorter wavelengths, as described in Ryzhkov and Zrnić (2007).

4. SUMMARY AND RECOMMENDATIONS

When they become available, the direct comparison of multiwavelength dual-polarization radar data will elucidate microphysical processes associated with severe storms and tornadoes. The important polarimetric signatures outlined above should be investigated by directly comparing polarimetric data from three radar wavelengths in an effort to better understand the cause and significance of these features. However, for a successful physical interpretation, quantitative analysis, and/or hydrometeor classification, data from shorter wavelengths must be properly corrected for attenuation and differential attenuation. Such correction techniques may not be straightforward but are critical for any analysis.

In addition to attenuation correction, calibrating the radar systems may be difficult. This is because the absolute values of the polarimetric variables will not be the same at each wavelength. We recommend a self-consistent calibration technique, but such a method may be difficult in supercells. In order to best perform a self-consistent calibration, widespread heavy (> 40 dBZ) rainfall is optimal. Thus, we recommend that data from a mesoscale convective system is collected for calibration purposes.

The effects of resonance scattering are extremely important, especially at shorter wavelengths. In addition to δ obfuscating the differential propagation phase, resonance-sized hydrometeors will contribute differently to the radar variables measured at different wavelengths. Identifying resonance scatterers at three wavelengths offers the possibility to better quantify the size of hydrometeors within the storm, offering important microphysical insight.

Finally, other data issues with short wavelength radars must be addressed. These include the look-angle correction for extremely close range observations, the increased prevalence of nonuniform beam filling effects, and the depolarization of the transmitted signal due to oriented crystals in the upper levels of the storm. Information gained from multiwavelength polarimetric data will be extremely enlightening, but a careful

analysis and control of the data quality is essential to maximize its benefits.

6. REFERENCES

Atlas, D. and F.H. Ludlam 1961: Multi-wavelength radar reflectivity of hailstorms. *Quart. J. Royal Meteor. Soc.*, **87**, 523-534.

Bluestein, H.B., M.M. French, R.L. Tanamachi, S. Frasier, K. Hardwick, F. Junyent, and A. Pazmany, 2007: Close-range observations of tornadoes in supercells made with a dual-polarization, X-band, mobile Doppler radar. *Mon. Wea. Rev.*, **135**, 1522-1543.

Bringi, V.N., V. Chandrasekar, N. Balakrishnan, and D.S. Zrnic, 1990: An examination of propagation effects in rainfall on radar measurements at microwave frequencies. *J. Atmos. Oceanic Technol.*, **7**, 829-840.

Bringi, V.N., T.D. Keenan, and V. Chandrasekar, 2001: Correcting C-band radar reflectivity and differential reflectivity data for rain attenuation: A self-consistent method with constraints. *IEEE Trans. Geosci. Remote Sens.*, **39**, 1906-1915.

Carey, L.D., S.A. Rutledge, D.A. Ahijevych, and T.D. Keenan, 2000: Correcting propagation effects in C-band polarimetric radar observations of tropical convection using differential propagation phase. *J. Appl. Meteor.*, **39**, 1405-1433.

Giangrande, S.E., 2002: Investigation of polarimetric measurements of rainfall at close and distant ranges. MS Thesis, Univ. of Oklahoma, 86 pp. [Available from School of Meteorology, University of Oklahoma, 120 David L. Boren Blvd., Norman, OK, 73072].

Heinselman, P.L. and A.V. Ryzhkov, 2006: Validation of polarimetric hail detection. *Wea. Forecasting*, **21**, 839-850.

Hubbert, J. and V.N. Bringi, 1995: An iterative filtering technique for the analysis of copolar differential phase and dual-frequency radar measurements. *J. Atmos. Oceanic Technol.*, **12**, 643-648.

Hubbert, J., V.N. Bringi, and L.D. Carey, 1998: CSU-CHILL polarimetric measurements from a severe hailstorm in eastern Colorado. *J. App. Meteor.*, **37**, 749-755.

Junyent, F., S. Frasier, D.J. McLaughlin, V. Chandrasekar, H.B. Bluestein, and M.M. French, 2005: High-resolution, dual-polarization radar observations of tornadoes: Implications for radar development and tornado detection. *Proc. Geosci. And Remote Sensing Symposium*, IEEE, **3**, 2034-2037.

Kumjian, M.R. and A.V. Ryzhkov, 2008: Polarimetric signatures in supercell thunderstorms *J. Appl. Meteor. and Climatol.*, **47**, 1940-1961.

Kumjian, M.R. and A.V. Ryzhkov, 2009: Storm-relative helicity revealed from polarimetric radar measurements. *J. Atmos. Sci.*, **in press.**

Kumjian, M.R., A.V. Ryzhkov, J.L. Alford, M. Knight, and J.W. Conway, 2008: Close range observations of a tornadic supercell with C-band polarimetric Doppler radar. *Extended Abstracts*, 88th Annual AMS Meeting, New Orleans, Amer., Meteor. Soc., P2.14.

Liu, Y., Y. Wang, D. Willie, V. Chandrasekar, and V.N. Bringi, 2007: Operational evaluation of the real-time attenuation correction system for CASA IP1 testbed. *Preprints*, 33rd Conf. on Radar Meteorology, Cairns, Australia, Amer. Meteor. Soc., P7.9.

Loney, M.L., D.S. Zrnić, J.M. Straka, and A.V. Ryzhkov, 2002: Enhanced polarimetric radar signatures above the melting level in a supercell storm. *J. Appl. Meteor.*, **41**, 1179-1194.

Lopez, F.J., A. Pazmany, H.B. Bluestein, M.R. Kramar, M.M. French, C. Weiss, and S. Frasier, 2004: Dual-polarization, mobile, X-band, Doppler radar observations of hook echoes in supercells. *Preprints*, 22nd Conf. on Severe Local Storms, Hyannis, MA, Amer. Meteor. Soc., CD-ROM, P11.7.

Outinen, K. and J. Teittinen, 2007: Case study of a tornadic supercell in Finland 28 August, 2005. *Extended Abstracts*, 4th European Conf. on Severe Storms, Trieste, Italy, CD-ROM.

Outinen, K. and J. Teittinen, 2008: Polarimetric radar observations of a tornadic supercell in Finland.

Extended Abstracts, 5th European Conf. on Radar in Meteorology and Hydrology, Helsinki, Finland, P4.3.

Payne, C.D., T.J. Schuur, D. Rust, D. MacGorman, M.I. Biggerstaff, K. Kuhlman, E. Bruning, and N. Lund, 2008: Electrical and polarimetric radar observations of a HP supercell on 29-30 May 2004 during TELEX. *Extended Abstracts*, 88th Annual Meeting, New Orleans, LA, Amer. Meteor. Soc., 4.6.

Romine, G.S., D.W. Burgess, and R.B. Wilhelmson, 2008: A dual-polarization radar based assessment of the 8 May 2003 Oklahoma City area tornadic supercell. *Mon. Wea. Rev.*, **136**, 2849-2870.

Ryzhkov, A.V., 2007: The impact of beam broadening on the quality of radar polarimetric data. *J. Atmos. Oceanic Technol.*, **24**, 729-744.

Ryzhkov, AV., D. Burgess, D. Zrnić, T. Smith, and S. Giangrande, 2002: Polarimetric analysis of a 3 May 1999 tornado. *Extended Abstracts*, 22nd Conf. Severe Local Storms, Hyannis, MA, Amer. Meteor. Soc., CD-ROM 14.2.

Ryzhkov, A.V., T.J. Schuur, D.W. Burgess, and D.S. Zrnić, 2005a: Polarimetric tornado detection. *J. Appl. Meteor.*, **44**, 557-570.

Ryzhkov, A.V., T.J. Schuur, D.W. Burgess, P.L. Heinselman, S.E. Giangrande, and D.S. Zrnić, 2005b: The joint polarization experiment. *Bull. Amer. Meteor. Soc.*, **86**, 809-824.

Ryzhkov, A.V., P. Zhang, D. Hudak, J.L. Alford, M. Knight, and J.W. Conway, 2007b: Validation of polarimetric methods for attenuation correction at C band. *Extended Abstracts*, 33rd Conf. Radar Meteorology, Cairns, Australia, Amer. Meteor. Soc., CD-ROM P11B.12.

Ryzhkov, A.V. and D.S. Zrnić, 1995: Precipitation and attenuation measurements at a 10-cm wavelength. *J. Appl. Meteor.*, **34**, 2121-2134.

Ryzhkov, A.V. and D.S. Zrnić, 2005: Radar polarimetry at S, C, and X bands. Comparative analysis and operational implications. Conf. 9R.3.

Ryzhkov, A.V., and D.S. Zrnić, 2007: Depolarization of ice crystals and its effect on radar polarimetric measurements. *J. Atmos. Oceanic Technol.*, **24**, 1256-1267.

Schlatter, P.T., 2003: Polarimetric radar and in-situ measurements of a nontornadic supercell. M.S. thesis, University of Oklahoma, 97 pp. [Available from School of Meteorology, University of Oklahoma, 120 David L. Boren Blvd., Norman, OK, 73072].

Schenkman, A.D., C.M. Shafer, and M.R. Kumjian, 2008: Multiplatform analysis of a tornadic convective system. *Extended Abstracts*, 5th European Conf. on Radar in Meteorology and Hydrology, Helsinki, Finland, P4.10.

Schuur, T.J., A.V. Ryzhkov, D.W. Burgess, and D.S. Zrnic, 2004: Polarimetric radar observations of tornadic debris signatures. *Preprints*, 22nd Conf. on Severe Local Storms, Hyannis, MA, Amer. Meteor. Soc., CD-ROM 14.2.

Snyder, J.C., 2008: Attenuation correction techniques and hydrometeor classification of high-resolution, X-band, dual-polarized mobile radar data of severe convective storms. M.S. Thesis, University of Oklahoma, 148 pp. [Available from School of Meteorology, University of Oklahoma, 120 David L. Boren Blvd., Norman, OK, 73072].

Testud, J., E. Le Bouar, E. Obligis, and M. Ali-Mehenni, 2000: The rain profiling algorithm applied to polarimetric weather radar. *J. Atmos. Oceanic Technol.*, **17**, 332-356.

Van Den Broeke, M. S., J.M. Straka, E.N. Rasmussen, 2008: Polarimetric radar observations at low-levels during tornado life cycles in a small sample of classic Southern Plains supercells. *J. App. Meteor. and Climatol.*, **47**, 1232-1247.

Van Vleck, J.H., 1947a: The absorption of microwaves by uncondensed water vapor. *Phys. Rev.*, **71**, 425-433.

Van Vleck, J.H., 1947b: Absorption of microwaves by oxygen. *Phys. Rev.*, **71**, 413-424.